Chemistry Europe
European Chemical Societies Publishing

Special Collection

The [1,2,4]Triazolo[4,3-*a*]pyridine as a New Player in the Field of IDO1 Catalytic Holo-Inhibitors

Silvia Fallarini,[a] Irene P. Bhela,[a] Silvio Aprile,[a] Enza Torre,[a] Alice Ranza,[a] Elena Orecchini,[b] Eleonora Panfili,[b] Maria T. Pallotta,[b] Alberto Massarotti,[a] Marta Serafini,*[a, c] and Tracey Pirali[a]

Inhibitors of indoleamine 2,3-dioxygenase 1 (IDO1) are considered a promising strategy in cancer immunotherapy as they are able to boost the immune response and to work in synergy with other immunotherapeutic agents. Despite the fact that no IDO1 inhibitor has been approved so far, recent studies have shed light on the additional roles that IDO1 mediates beyond its catalytic activity, conferring new life to the field. Here we present a novel class of compounds originated from a structure-based virtual screening made on IDO1 active site. The starting hit compound is a novel chemotype based on a [1,2,4]triazolo[4,3-*a*]pyridine scaffold, so far underexploited among the heme binding moieties. Thanks to the rational and *in silico*-guided design of analogues, an improvement of the potency to sub-micromolar levels has been achieved, with excellent *in vitro* metabolic stability and exquisite selectivity with respect to other heme-containing enzymes.

Introduction

Among the eight hallmarks of cancer,[1–3] the escape of tumoral cells from the immune surveillance is currently drawing considerable attention. Immunotherapy has undoubtedly revolutionized the clinical outcome of certain types of cancer, but insufficient response rates due to acquired or innate immune resistance are still an unsolved issue.[4–6]

Therefore, compounds able to boost the immune response by targeting different mechanisms of tumoral immunosuppression are considered as a promising strategy to enhance the efficacy of existing immunotherapeutic drugs.[7,8] Among the possible combinatorial strategies, indoleamine 2,3-dioxygenase 1 (IDO1) has emerged as an attractive target due to its crucial role in the maintenance of a balance between immune tolerance and immunity.[9] The overexpression of IDO1 in the tumour microenvironment leads to a dysregulation of this balance, and to an escape of the tumour cells from immune control, a feature that is associated with poor prognosis[10] and metastatic progression.[11] For years, the molecular mechanism underlying this process has been exclusively related to the catalytic activity of IDO1, represented by the conversion of tryptophan (Trp) into kynurenines (Kyn) in the first and rate-limiting step of the kynurenine pathway.[12,13] However, additional functions of IDO1 have been elucidated over recent years, highlighting that the role of this protein is far more complicated than initially believed. To name a few recent discoveries, IDO1 (i) is a moonlighting protein possessing a signalling activity and able to interact with molecular partners, resulting in the upregulation of its gene expression or in its degradation by the proteasomal system,[14–16] (ii) has a nitrite reductase activity under hypoxia and induces the chemical reduction of nitrite to nitric oxide,[17] (iii) in cells, is present as an equilibrium between the catalytically active form (holo) and the heme-free apo-form, depending on the availability of heme group and Trp,[18,19] (iv) produces singlet molecular oxygen in arterial endothelial cells under inflammatory conditions, contributing to blood pressure control.[20] Not surprisingly, therefore, the design of IDO1 inhibitors is a highly dynamic field, with thousands of molecules reported in the literature,[21] several clinical candidates under development[22] and different mechanisms of action described.[23] Undoubtedly, the failure of the Phase III clinical trial of epacadostat, the most promising candidate until three years ago, represented a serious setback in the field,[24–26] but in the meanwhile, other inhibitors have entered the clinical phases and at least one candidate (linrodostat, BMS-986204)[27] is currently evaluated in Phase III,[28] rekindling enthusiasm in the field. Additional efforts are currently put in place to identify either molecules able to inhibit the hitherto overlooked activities of IDO1 or novel chemotypes endowed with improved properties.

[a] Dr. S. Fallarini, I. P. Bhela, Dr. S. Aprile, Dr. E. Torre, A. Ranza, Prof. A. Massarotti, Dr. M. Serafini, Prof. T. Pirali
Department of Pharmaceutical Sciences
Università degli Studi del Piemonte Orientale
Largo Donegani 2, 28100 Novara (Italy)
E-mail: marta.serafini@uniupo.it
[b] E. Orecchini, Dr. E. Panfili, Dr. M. T. Pallotta
Department of Medicine and Surgery
University of Perugia, Perugia, 06132 (Italy)
[c] Dr. M. Serafini
Current address: Department of Chemistry
Chemistry Research Laboratory
University of Oxford
Mansfield Road, Oxford OX1 3TA (UK)

Supporting information for this article is available on the WWW under https://doi.org/10.1002/cmdc.202100446

This article belongs to the Early-Career Special Collection, "EuroMedChem Talents".

Our research group contributed to the IDO1 field with the publication of three classes of inhibitors, based on imidazole,[29] imidazothiazole[30,31] and benzimidazole scaffolds.[32] The latter class emerged from a structure-based virtual screening that was performed on ZINC15 database[33] by mining more than 8 million molecules in IDO1 active site. The 500 compounds with the highest score according to their predicted pose in the active site were further evaluated by visual inspection and 50 of them were selected and purchased from eMolecules®,[34] a website collecting in-stock or synthesised compounds from global suppliers, and tested. First, an MTT assay was performed to rule out an intrinsic cytotoxicity: cell viability was measured after 48 hours in the presence of the selected compounds at 10 μM. Then, IDO1 inhibition was assessed in melanoma derived human A375 cell line which expressed high levels of the enzyme after induction by recombinant human IFN-γ. Cells were treated with 10 μM of the compounds for 48 hours and L-Kyn reduction was detected by HPLC analysis and compared to the basal levels. Following this protocol, 7 hit compounds out of 50, which were not structurally related, were identified with IC_{50} values spanning from 4.4 to 0.016 μM.

The most potent hit compound, VS13 (**1**, Figure 1), displays a low nanomolar potency over a panel of different tumoral cell lines and has a remarkable *in vivo* pharmacodynamic activity, despite the metabolic liability.[32] Besides VS13, a second hit compound, named VS9 (**2**, Figure 1), was identified with an IC_{50} value in the low micromolar range (2.6 μM). Interestingly, it is based on a novel chemotype, not shared by other IDO1 inhibitors already reported, namely a [1,2,4]triazolo[4,3-*a*] pyridine substructure. While 1,2,4-triazoles are well known to bind the heme group, as exemplified by many antifungal agents,[35] very few IDO1 inhibitors with this substructure have been identified so far. In particular, among the iron-binding scaffolds with sub-micromolar potency, imidazoles (*e.g.* 4-phenylimidazole),[36] hydroxyamidines (*e.g.* epacadostat),[37] indazoles,[38–40] and 1,2,3-triazoles[41] are the most exploited ones, while 1,2,4-triazole-based inhibitors are less represented and comprise Amg-1 (**3**, Figure 1),[42] a thiazolo[2,3-*c*][1,2,4] triazole, and the recently reported 3-monosubstitued 1,2,4-triazole (**4**, Figure 1).[43] The under-representation of this substructure in the literature caught our attention and prompted us to start a medicinal chemistry campaign on VS9.

Results and Discussion

To confirm the biological activity of the purchased hit compound, VS9 was resynthesized in our lab, exploiting a four-step synthetic route. As depicted in Scheme 1, after reaction between **5** and Boc-glycine **6**, the resulting intermediate **7** was cyclized in the presence of Lawesson's reagent and the Boc group was removed. The resulting amine **9** is very polar and difficult to be extracted from aqueous phase during workup. The reaction mixture was therefore directly subjected to column chromatography using EtOAc to remove trifluoroacetic acid (TFA) and EtOAc/MeOH 7:3 to elute the trifluoroacetate salt of amine **9**, with a yield of 58%. This procedure was next applied to the synthesis of the other amines reported below. Finally, amine **9** was coupled with 1*H*-indazole-7-carboxylic acid, yielding VS9 (**2**). The synthesized hit compound was then re-tested for IDO1 inhibition in A375 cell line at 10 μM, cytotoxicity and IC_{50} value and the results were comparable to those obtained with the purchased molecule (Table 1). Moreover, as the indazole moiety of VS9 resembles the structure of a previously reported apo-inhibitor,[44] to ascertain the inhibition of the holo-IDO1 rather than the apo form, the compound was also tested on an enzyme-based assay using the recombinant form of human IDO1 (rhIDO1). rhIDO1 was treated with 10 μM of VS9 and the conversion of L-Trp to L-Kyn was determined spectrophotometrically using *p*-dimethylaminobenzaldehyde. While apo inhibitors show a lack of inhibition in the enzyme-based assay in face of a high cellular activity,[18,19,45] VS9 provided an rhIDO1 inhibition of 54.6 ± 3.1% (see also Supporting Information), comparable to the result from the cellular-based assay. To further confirm the absence of binding to the apo-form, the interference of the compound with the amount of free heme produced after incubation with IDO1 was evaluated.[19] Similarly to epacadostat, VS9 did not increase the

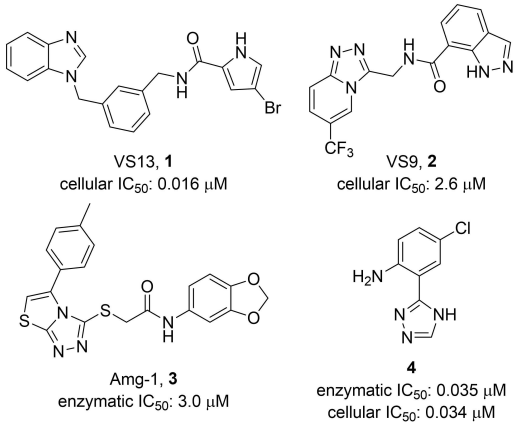

Figure 1. Structures of selected IDO1 inhibitors.

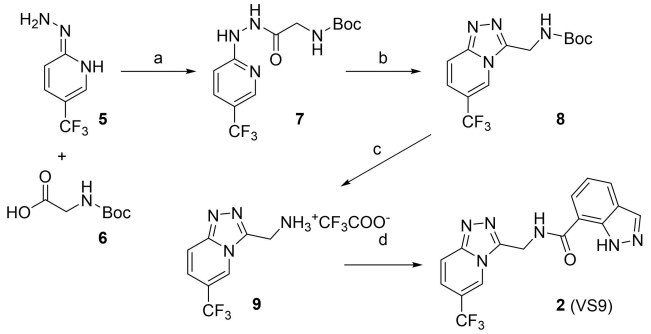

Scheme 1. Preparation of VS9 (**2**): (a) NMM, isobutyl chloroformate, THF, 0 °C, 18 h, 80%. (b) Lawesson's reagent, DME, 80 °C, 7 h, 99%. (c) TFA, CH_2Cl_2, 0 °C, 2 h, 58%. (d) 1*H*-Indazole-7-carboxylic acid, EDCI, HOBt, TEA, dry CH_2Cl_2, dry DMF, rt, 18 h, 44%.

Table 1. VS9 analogues with modifications of the substructure putatively located in pocket B.[a]

Cpd, Yield (%)	Cell viability [%] @ 10 μM ± SD	IDO cellular assay inhibition [%] @ 10 μM ± SD	IC_{50} ± SD [μM], A375 cell line
VS9	91 ± 9.9	35 ± 6	2.6 ± 0.5
2, 44	87 ± 18.3	42 ± 9	2.8 ± 0.9
10, 76	90 ± 14.8	34 ± 1	–
11, 67	91 ± 12.7	22 ± 5	–
12, 46	92 ± 12	40 ± 8	–
13, 40	94 ± 2.8	32 ± 7	–
14, 49	100 ± 0	38 ± 1	–
15, 64	100 ± 0.7	11 ± 1	–
16, 68	100 ± 5.2	19 ± 3	–
17, 47	89 ± 9.2	43 ± 10	–
18, 62	88 ± 16.8	29 ± 2	–
19, 63	97 ± 2.1	24 ± 5	–
20, 65	100 ± 0	31 ± 29	–
21, 60	78 ± 4.2	49 ± 15	–
22, 42	93 ± 9.8	39 ± 4	–
24, 48	95 ± 7.2	75 ± 7	2.0 ± 0.3
25, 37	94 ± 2.1	79 ± 4	1.4 ± 0.5

[a] Cytotoxicity and IDO1 inhibition in A375 cell line at 10 μM and cellular IC_{50} values. The reported values derive for three independent experiments and numbers represent mean ± standard error of mean (SEM).

levels of free heme (see Supporting Information), confirming the molecule as a catalytic holo-inhibitor.

A SAR study based on this scaffold was then undertaken. As shown in Figure 2, the docking pose of the compound sees the 6-(trifluoromethyl)-[1,2,4]triazolo[4,3-*a*]pyridine moiety accommodated in pocket A (Tyr126, Cys129, Val130, Phe163, and Phe164),[46] with one of the nitrogen atoms of the triazole ring responsible for the coordination with the iron of the heme group. Pocket B (Phe226, Arg231 and Ser235)[46] is occupied by the indazole moiety, while pocket C (Gly236, Lys238, Ala260, Gly261, Gly262, Ser263, Phe291, Met295),[30] a distal hydrophobic region located near the solvent region, is not exploited. Next, Molecular Dynamics (MD) simulation using the Desmond package was used to further analyse the docking results of VS9.[47] The MD of IDO1/VS9 complex was simulated for 100 ns at 300 K using a standard protocol. The coordinates of the IDO1 Cα and the ligand of each MD timesteps were compared to the original coordinates (see Supporting Information) and the root mean square deviations (RMSDs) showed that the protein-ligand structure was stabilized. The results obtained from the MD simulation are consistent with the predicted docking pose: the 6-(trifluoromethyl)-[1,2,4]triazolo[4,3-*a*]pyridine moiety is stabilized in pocket A where it interacts with the heme group for most of the time, while the indazole group is located in pocket B for the entire duration of the simulation, interacting with Phe226.

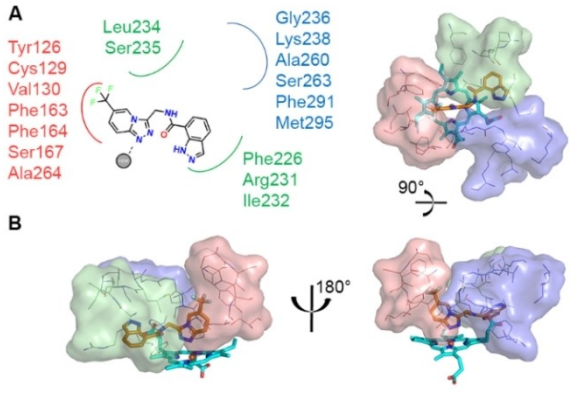

Figure 2. Docking pose of the hit compound VS9. A) Schematic representation of predicted interactions of VS9 within IDO1 binding pockets. B) Docking pose of VS9. Amino acids of pocket A, pocket B, and pocket C are depicted in red, green, and blue, respectively. The heme group and VS9 are depicted as cyan and orange sticks, respectively.

Initially, we focused our attention on the modification of the portion putatively located in pocket B and we varied the indazole moiety by exploiting coupling reactions among amine **9** and different carboxylic acids. The synthesis of these analogues was guided *in silico*[48–50] to increase the possibility to find effective inhibitors and to maximize the interaction in IDO1 active site. To this aim, synthetically feasible and purchasable carboxylic acids were virtually combined to generate a small library of candidates that was screened in the IDO1 active site. The virtual candidates were then docked in IDO1 binding site and ranked according to their binding energy. Those displaying the highest score were selected and synthesized, according to Scheme 2. This effort led to the first series of analogues, **10**–**22**, which were then biologically tested. First, cell viability was evaluated in the presence of 10 μM of the compounds of interest after 48 hours. All the compounds did not significantly affect cell viability and were then evaluated for IDO1 inhibition as described above. Within the first series, 3 compounds

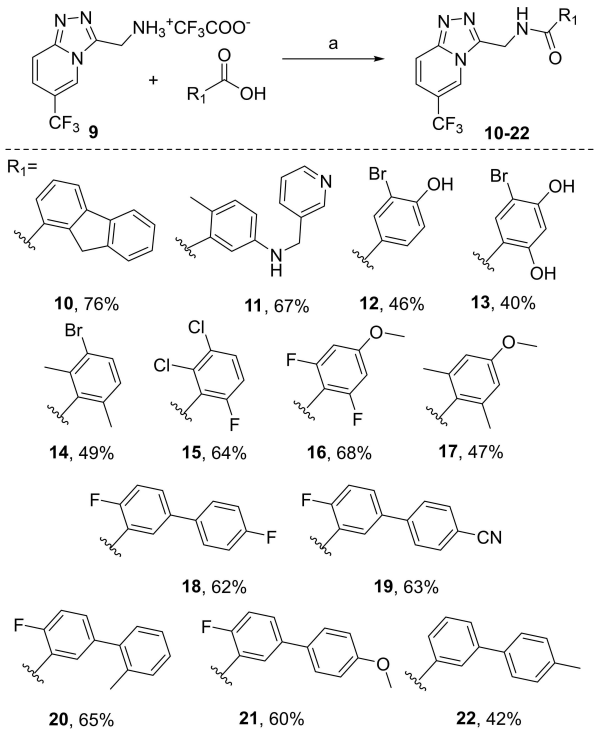

Scheme 2. Preparation of 6-(trifluoromethyl)-[1,2,4]triazolo[4,3-*a*]pyridine-based VS9 analogues **10**–**22**: (a) EDCI, HOBt, TEA, dry CH_2Cl_2, dry DMF, rt, 18 h, 40–76%.

retained an IDO1 inhibition comparable to VS9 (**12**, **17**, **21**, Table 1).

Based on these results, a second series of analogues was *in silico* designed starting from the structure of the 4 most active molecules (**2**, **12**, **17**, **21**, Table 1). To evaluate the binding pose of each molecule, an initial water network in the binding site was created around the structure of the compounds using SZMAP/GAMEPLAN.[51] As protein-ligand binding interactions occur in an aqueous environment, by using SZMAP calculations significant thermodynamic favourable or unfavourable regions of solvent in the binding site were identified. GAMEPLAN analyses the results to suggest ways to modify ligand chemistry based on the water structure in the immediate environment of the ligand. The molecular surfaces were then visualized using VIDA,[52] and structural modifications were visually selected with the aim of further improving the activity.

The portion of compound **21** which is putatively located in pocket B tolerated the insertion of a second methoxy substituent in ortho to the methoxy group or the substitution of both methoxy substituents with two methyl. The two corresponding analogues, **24** and **25**, were therefore synthesized using an alternative synthetic route (Scheme 3), as the required carboxylic acids for these products were not commercially available. Intermediate **23** was obtained *via* coupling reaction from amine **9** and then two Suzuki cross-coupling reactions were performed, affording **24** and **25** (Scheme 3).

From the VIDA visualization of the molecular surfaces of the portion in pocket A,[52] it was highlighted that the $-CF_3$ group could be either substituted with a halogen atom or a phenyl ring fused to the [1,2,4]triazolo[4,3-*a*]pyridine system. To this aim, two additional amines, **29** and **36**, were synthesized according to Schemes 4 and 5. In both cases, the synthetic routes resembled the one exploited for amine **9**. The carboxylic acids were selected from those affording the highest inhibitory activity among compounds **2**, **10**–**22**, **24**–**25** (Table 1).

From amine **29**, compound **30** was obtained by coupling reaction, while compound **32** was prepared by amidation using 2-fluoro-5-iodobenzoic acid followed by Suzuki reaction (Scheme 4). Four compounds (**37**–**40**) were obtained by amidation from amine **36** (Scheme 5). One candidate (**42**), in which the $-CF_3$ group is absent, was synthesized by coupling reaction between the commercially available amine **41** and 1*H*-indazole-7-carboxylic acid (Scheme 5). Finally, compound **44** was synthesized with the aim of validating the predicted interaction with heme group in pocket A by one of the nitrogen atoms of the triazole ring. The molecule was obtained by reacting the commercially available amine **43** with 1*H*-indazole-7-carboxylic acid (Scheme 5).

Compounds **24**–**25** (Table 1), **30**, **32**, **37**–**40**, **42** and **44** (Table 2) were evaluated as described for the first series of analogues for cell cytotoxicity and IDO1 inhibition.

Gratifyingly, the compounds from the second series afforded a higher inhibition compared to the first one, with 6 molecules that display a percentage of inhibition higher than

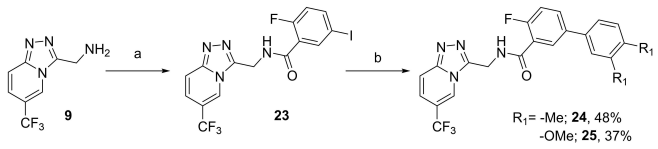

Scheme 3. Preparation of 6-(trifluoromethyl)-[1,2,4]triazolo[4,3-*a*]pyridine-based VS9 analogues **24**–**25**: (a) EDCI, HOBt, TEA, dry CH_2Cl_2, dry DMF, rt, 18 h, 70%. (b) R_2-$B(OH)_2$, EtOH, dry DMF, $Pd(OAc)_2$, K_2CO_3, 80 °C, 32 h, 37–48%.

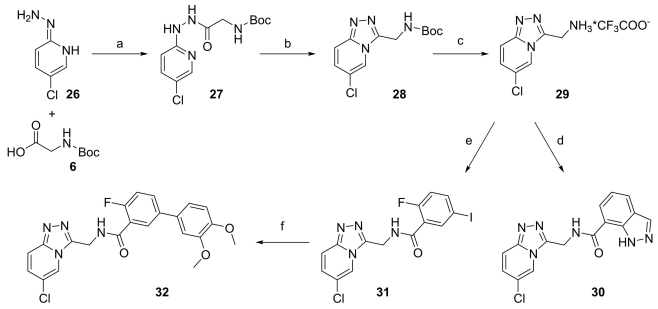

Scheme 4. Preparation of 6-chloro-[1,2,4]triazolo[4,3-*a*]pyridine-based VS9 analogues **30** and **32**: (a) NMM, isobutyl chloroformate, THF, 0 °C, 3 h, 69%. (b) Lawesson's reagent, DME, 80 °C, 2 h, 92%. (c) TFA, CH_2Cl_2, 0 °C, 2 h, 40%. (d) 1*H*-Indazole-7-carboxylic acid, EDCI, HOBt, TEA, dry CH_2Cl_2, dry DMF, rt, 18 h, 42%. (e) 2-Fluoro-5-iodobenzoic acid, EDCI, HOBt, TEA, dry CH_2Cl_2, dry DMF, rt, 18 h, 40%. (f) (3,4-Dimethoxyphenyl)boronic acid, EtOH, dry DMF, $Pd(OAc)_2$, K_2CO_3, 80 °C, 32 h, 70%.

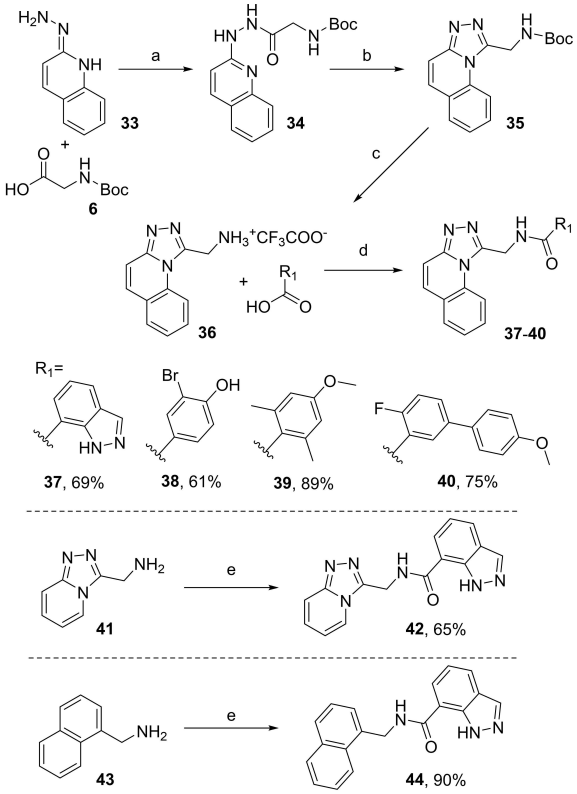

Scheme 5. Preparation of VS9 analogues **37**–**40**, **42** and **44**: (a) NMM, isobutyl chloroformate, THF, 0 °C, 18 h, 84%. (b) Lawesson's reagent, DME, 80 °C, 6 h, 80%. (c) TFA, CH_2Cl_2, 0 °C, 2 h, 54%. (d) EDCI, HOBt, TEA, dry CH_2Cl_2, dry DMF, rt, 18 h, 61–89%. (e) 1*H*-Indazole-7-carboxylic acid, EDCI, HOBt, TEA, dry CH_2Cl_2, dry DMF, rt, 18 h, 65–90%.

Table 2. VS9 analogues with modifications of the substructure putatively located in pocket A.[a]

Cpd, Yield (%)	Cell viability [%] @ 10 μM ± SD	IDO cellular assay inhibition [%] @ 10 μM ± SD	IC_{50} ± SD [μM], A375 cell line
VS9	91 ± 9.9	35 ± 6	2.6 ± 0.5
2, 44	87 ± 18.3	42 ± 9	2.8 ± 0.9
30, 42	98 ± 7.4	23 ± 5	–
32, 70	98 ± 9.3	24 ± 5	–
37, 69	100 ± 4.1	64 ± 8	6.9 ± 0.8
38, 61	95 ± 7.1	53 ± 7	0.9 ± 0.02
39, 89	94 ± 6.3	55 ± 6	1.8 ± 0.2
40, 75	97 ± 3.8	67 ± 9	3.4 ± 0.3
42, 65	100 ± 0	1 ± 1	–
44, 90	99 ± 1	2 ± 2	–

[a] Cytotoxicity and IDO1 inhibition in A375 cell line at 10 μM and cellular IC_{50} values. The reported values derive for three independent experiments and numbers represent mean ± standard error of mean (SEM).

50%. The highest inhibition is afforded by the biphenyl analogues **24** and **25** and the [1,2,4]triazolo[4,3-*a*]quinoline derivatives **37**–**40**, while 6-chloro-[1,2,4]triazolo[4,3-*a*]pyridine-based compounds possess only poor activity (**30**, **32**) and a completely drop in the activity is observed when the $-CF_3$ group is removed (**42**) highlighting that the presence of a hydrophobic substituent in this position is fundamental for the interaction within pocket A. Compound **44**, in which the [1,2,4]triazolo[4,3-*a*]pyridine is substituted with a naphthalene group is devoid of activity, suggesting a lack of interaction of this compound with the heme group. Interestingly, the indazole group can potentially drive the iron-binding,[21,38–40] but the lack of activity of compound **44** suggests that the preferential pose for VS9 analogues does not favour the interaction of this moiety with pocket A. This hypothesis is also supported by the MD simulation in which the indazole moiety of VS9 is stabilized in pocket B for the entire duration of the simulation (Figure 2).

The 6 compounds displaying an IDO1 inhibitory activity higher than 50% (**24**, **25**, Table 1 and **37**, **38**, **39**, **40**, Table 2) were selected and the IC_{50} values were calculated. Gratifyingly, 4 compounds (**24**, **25**, **38**, **39**, Table 1 and 2) are more potent than the precursor, with one candidate displaying an IC_{50} value in the nanomolar level (**38**, 0.9 μM, Table 2).

As the metabolic reaction catalysed by IDO1 is also mediated by tryptophan 2,3-dioxygenase (TDO),[53] the compounds were evaluated for their selectivity over TDO. Despite both enzymes are heme-containing dioxygenases, the two proteins share only 10% sequence identity and, while TDO is a tetramer, IDO1 is a monomer. To this aim, VS9 and its analogues (**24**, **25**, **38**, **39**) were tested in a mastocytoma cell line (P1.HTR) which does not expressed dioxygenases, but was stably transfected with a vector coding for human IDO1 (P1.IDO1) or TDO (P1.TDO).[32] Cells were treated with a 10 μM solution of each candidate for 16 h and L-Kyn secretion in cell culture supernatants was detected by HPLC analysis. The compounds were not able to induce a reduction of Kyn levels in P1.TDO compared to P1.IDO1, pointing at the molecules as selective IDO1 inhibitors (see Supporting Information for related figures).

The most potent analogues were then evaluated for their *in vitro* metabolic stability. The class, indeed, shares a non-hindered amide moiety which can be putatively susceptible toward hydrolytic metabolism, as previously observed for other IDO1 inhibitors.[54,55] To rule out this possibility, the candidates (**2**, **24**, **25**, **38**, **39**, **40**) were incubated for 1 h in rat liver S9 fraction (RLS9) supplied with NADPH and then the residual substrate was measured. Under these conditions, the compounds showed an excellent metabolic stability, with residual substrates higher than 99% (see Supporting Information for full data). The metabolite analysis was performed by liquid chromatography coupled to high-resolution tandem mass spectrometry (LC-$HRMS^2$, see Supporting Information for metabolite profiling and LC-$HRMS^2$ conditions) monitoring a list of ions corresponding to those of the expected metabolites. Despite the presence of the non-steric hindered amide group, this moiety is exceptionally stable toward hydrolysis. Furthermore, oxidative metabolism was revealed to be NADPH-dependent, suggesting the involvement of the hepatic monooxygenase system. Indeed, the main metabolic pathways are represented by aliphatic, aromatic hydroxylation, and *O*-demethylation.

Finally, the scaffold of 1,2,4-triazole on which this class is based is particularly abundant in antifungal agents. These drugs are known for their ability to interfere with the mammalian cytochrome P450, potentially leading to adverse reactions related to drug-drug interactions. To predict the binding to the CYP enzymes, the 2 most potent compounds, **25** and **38**, were evaluated in an aminopyrine *N*-demethylase assay at a concentration of 1, 10 and 100 μM (see Supporting Information). Compared to ketoconazole, a well-known antifungal CYP3A4 inhibitor which induced a strong inhibition of CYP, **25** showed a low inhibition at 10 and 100 μM, while **38** did not significantly inhibit CYP at the tested concentrations.

Conclusion

Starting from a hit compound, VS9, identified by means of a structure-based virtual screening and representing an unprecedented chemotype, a class of [1,2,4]triazolo[4,3-*a*]pyridine-based analogues was *in silico* designed and synthesized. As demonstrated by the SAR study and the performed molecular dynamics, the coordination with the iron atom of the heme group is driven by the N1 atom of the 1,2,4-triazole ring, underexploited in the field of IDO1 inhibitors. The synthetic efforts have led to **38** that shows an IC_{50} value of 0.9 μM, a high selectivity over TDO and CYPs and no detectable cytotoxicity up to 10 μM. The compound is also cell-permeable and fully stable toward *in vitro* hepatic metabolism, representing a promising starting point in the generation of new IDO1 inhibitors.

For example, to capitalize upon the newly described [1,2,4]triazolo[4,3-*a*]pyridine scaffold, the elongation of the side chain located in pocket B might represent a strategy to achieve additional interaction with the distal pocket C[30,32] and further improve the potency of this class of molecules.

Experimental Section

Chemistry

Commercially available reagents and solvents were used as purchased without further purification. When needed, solvents were distilled and stored on molecular sieves. Column chromatography was performed on silica gel. Thin layer chromatography (TLC) was carried out on 5 cm × 20 cm plates with a layer thickness of 0.25 mm. When necessary, TLC plates were visualized with aqueous $KMnO_4$ or with aqueous solution of cerium (IV) sulfate and ammonium molybdate in sulfuric acid. Melting points were determined in open glass capillary with a Stuart scientific SMP3 apparatus. All the target compounds were checked by IR (FT-IR Bruker Alpha II), ^{1}H-NMR (Bruker Avance Neo 400 MHz), ^{13}C-NMR (Bruker Avance Neo 400 MHz), and mass spectrometry (Thermo Scientific Q-Exactive Plus) equipped with an HESI source. Chemical shifts are reported in parts per million (ppm).

General procedure for the synthesis of compounds 2, 10–23

Amine **9** (230 mg, 0.70 mmol) was solubilized in dry CH_2Cl_2 (4 mL) under nitrogen. TEA (109 μL, 0.76 mmol), HOBt (56.3 mg, 0.42 mmol), EDCI (79.8 mg, 0.42 mmol) and carboxylic acid (0.35 mmol, 1 eq) were added in order. The reaction was stirred at room temperature overnight, then diluted with CH_2Cl_2 and washed with water (3x). The organic layer was dried over sodium sulfate and evaporated. Purification by silica gel column chromatography afforded compounds **2**, **10**–**23**.

N-((6-(Trifluoromethyl)-[1,2,4]triazolo[4,3-a]pyridin-3-yl) methyl)-1H-indazole-7-carboxamide, (2)

PE/EtOAc 1:9. Yellowish solid. Yield 44%; mp: 215–217 °C. ^{1}H-NMR (400 MHz, DMSO-d_6): δ 13.05 (br s, 1H), 9.45 (br s, 1H), 9.28 (s, 1H), 8.17 (s, 1H), 8.00–7.96 (m, 3H), 7.62 (d, J = 9.1 Hz, 1H), 7.21 (t, J = 8.0 Hz, 1H), 5.18 (s, 2H). ^{13}C-NMR (101 MHz, DMSO-d_6): δ 166.9, 149.4, 147.0, 134.6, 129.2, 128.2, 127.2, 125.6, 125.4, 124.7, 123.5, 120.2, 119.4, 116.5, 110.3, 33.8. IR (neat): $\tilde{\nu}$ = 3343, 3233, 3101, 3042, 2923, 2853, 1299, 1131, 742 cm^{-1}. MS (ESI): m/z 359 $[M–H]^-$. HRMS (ESI) m/z $(M+H)^+$ calcd for $C_{16}H_{12}F_3N_6O$ 361.1019, found 361.1026.

N-((6-(Trifluoromethyl)-[1,2,4]triazolo[4,3-a]pyridin-3-yl) methyl)-9H-fluorene-4-carboxamide, (10)

PE/EtOAc 2:8. White solid. Yield 76%; mp: 216–218 °C. ^{1}H-NMR (400 MHz, DMSO-d_6): δ 9.39 (br t, J = 5.5 Hz, 1H), 9.33 (s, 1H), 8.04 (d, J = 9.7 Hz, 1H), 7.67–7.76 (m, 2H), 7.57 (d, J = 7.5 Hz, 1H), 7.52 (d, J = 7.8 Hz, 1H), 7.36–7.33 (m, 2H), 7.28 (t, J = 7.5 Hz, 1H), 7.05 (t, J = 7.5 Hz, 1H), 5.19 (d, J = 5.8 Hz, 2H), 3.93 (s, 2H).^{13}C-NMR (101 MHz, DMSO-d_6): δ 170.1, 149.5, 146.9, 144.5, 144.0, 139.9, 137.7, 131.7, 127.5, 126.8 (q, J = 4.5 Hz), 126.6, 126.1, 125.8 (q, J = 6.0 Hz), 125.4, 125.2, 124.2 (q, J = 250 Hz), 123.6, 122.6, 117.3, 116.2 (q, J = 33.4 Hz), 36.8, 33.7. IR (neat): $\tilde{\nu}$ = 3226, 3040, 2924, 2853, 1651, 1524, 1321, 1121, 880, 734 cm^{-1}. MS (ESI): m/z 409 $[M+H]^+$. HRMS (ESI) m/z $(M+H)^+$ calcd for $C_{22}H_{16}F_3N_4O$ 409.1271, found 409.1261.

2-Methyl-3-((pyridin-3-ylmethyl)amino)-N-((6-(trifluoromethyl)-[1,2,4]triazolo[4,3-a]pyridin-3-yl)methyl) benzamide, (11)

EtOAc/MeOH 98:2. Amorphous white solid. Yield 67%. ^{1}H-NMR (400 MHz, $(CD_3)_2CO$): δ 9.38 (s, 1H), 8.61 (s, 1H), 8.43 (d, J = 6.4 Hz, 1H), 8.23 (br s, 1H), 7.90 (d, J = 9.6 Hz, 1H), 7.74 (d, J = 7.9 Hz, 1H), 7.58 (dd, J_s = 9.7, 1.7 Hz, 1H), 7.28 (dd, J_s = 8.6, 3.9 Hz, 1H), 6.96 (t, J = 7.9 Hz, 1H), 6.69 (d, J = 7.6 Hz, 2H), 6.59 (d, J = 8.2 Hz, 2H), 5.22 (d, J = 6.1 Hz, 2H), 4.51 (s, 2H), 2.91 (br s, 1H), 2.22 (s, 3H). ^{13}C-NMR (101 MHz, $(CD_3)_2CO$): δ 171.2, 149.5, 149.0, 148.1, 146.8, 146.4, 137.2, 135.5, 134.6, 126.2, 125.1 (q, J = 6.1 Hz), 123.8 (q, J = 269.9 Hz), 123.3, 122.6, 119.8, 117.0, 116.8 (q, J = 33.5 Hz), 115.4, 111.2, 44.7, 33.3, 13.1. IR (neat): $\tilde{\nu}$ = 3370, 3046, 1630, 1530, 1316, 1119, 791, 709 cm^{-1}. MS (ESI): m/z 441 $[M+H]^+$. HRMS (ESI) m/z $(M+H)^+$ calcd for $C_{22}H_{20}F_3N_6O$ 441.1645, found 441.1636.

3-Bromo-4-hydroxy-N-((6-(trifluoromethyl)-[1,2,4]triazolo [4,3-a]pyridin-3-yl)methyl)benzamide, (12)

PE/EtOAc 2:8. White solid. Yield 46%; mp: 271–273 °C. ^{1}H-NMR (400 MHz, DMSO-d_6): δ 9.25 (s, 1H), 9.16 (br s, 1H), 8.04 (d, J = 2.2 Hz, 1H), 7.98–7.94 (m, 2H), 7.74 (dd, J_s = 8.6, 2.2 Hz, 1H), 7.61 (dd, J_s = 9.7, 1.7 Hz, 1H), 6.99 (br d, J = 8.6 Hz, 1H), 5.04 (d, J = 5.6 Hz, 2H). ^{13}C-NMR (101 MHz, DMSO-d_6): δ 165.9, 157.6, 149.4, 147.1, 132.7, 129.0, 126.1, 125.8 (q, J = 6.3 Hz), 124.1 (q, J = 320 Hz), 123.5, 117.2, 116.4, 116.2 (q, J = 33.6 Hz), 109.5, 33.8. IR (neat): $\tilde{\nu}$ = 3285, 3054, 2922, 2724, 2592, 1656, 1601, 1539, 887, 703 cm^{-1}. MS (ESI): m/z 415 $[M+H]^+$. HRMS (ESI) m/z $(M+H)^+$ calcd for $C_{15}H_{11}BrF_3N_4O_2$ 415.0012, found 415.0004.

5-Bromo-2,4-dihydroxy-N-((6-(trifluoromethyl)-[1,2,4]triazolo [4,3-a]pyridin-3-yl)methyl)benzamide, (13)

PE/EtOAc 2:8. White solid. Yield 40%; mp: 196–198 °C. ^{1}H-NMR (400 MHz, DMSO-d_6): δ 9.31 (br s, 1H), 9.25 (s, 1H), 8.04–7.98 (m, 2H), 7.65–7.60 (m, 2H), 6.50 (br s, 2H), 5.08 (d, J = 5.4 Hz, 2H). ^{13}C-NMR (101 MHz, DMSO-d_6): δ 168.5, 161.1, 159.1, 146.6, 145.3, 132.7, 127.1, 125.7 (q, J = 6.0 Hz), 123.9 (q, J = 272 Hz), 123.7, 123.5, 117.2, 116.3 (q, J = 33.7 Hz), 109.0, 33.8. IR (neat): $\tilde{\nu}$ = 3211, 2922, 2852, 1742, 1586, 1558, 1234, 1126, 832, 821, 741 cm^{-1}. MS (ESI): m/z 431 $[M+H]^+$. HRMS (ESI) m/z $(M+H)^+$ calcd for $C_{15}H_{11}BrF_3N_4O_3$ 430.9961, found 430.9952.

3-Bromo-2,6-dimethyl-N-((6-(trifluoromethyl)-[1,2,4]triazolo [4,3-a]pyridin-3-yl)methyl)benzamide, (14)

PE/EtOAc 4:6. Colourless oil. Yield 49%. ^{1}H-NMR (400 MHz, $(CD_3)_2CO$): δ 9.34 (s, 1H), 8.42 (br s, 1H), 7.90 (d, J = 9.6 Hz, 1H), 7.61 (dd, J_s = 9.6, 1.8 Hz, 1H), 7.46 (d, J = 8.2 Hz, 1H), 6.98 (d, J = 8.2 Hz, 1H), 5.29 (d, J = 6.1 Hz, 2H), 2.25 (s, 3H), 2.15 (s, 3H). ^{13}C-NMR (101 MHz, $(CD_3)_2CO$): δ 169.6, 149.5, 146.5, 139.3, 133.9, 133.5, 132.4, 129.1, 125.0 (q, J = 6.0 Hz), 123.4 (q, J = 268.8 Hz), 122.8, 122.0, 117.0, 116.8 (q, J = 33.9 Hz), 33.1, 19.1, 18.0. IR (neat): $\tilde{\nu}$ = 3233, 3050, 2928, 1652, 1531, 1129, 809, 734 cm^{-1}. MS (ESI): m/z 427 $[M+H]^+$. HRMS (ESI) m/z $(M+H)^+$ calcd for $C_{17}H_{15}BrF_3N_4O$ 427.0376, found 427.0368.

2,3-Dichloro-6-fluoro-N-((6-(trifluoromethyl)-[1,2,4]triazolo [4,3-a]pyridin-3-yl)methyl)benzamide, (15)

PE/EtOAc 2:8. White solid. Yield 64%; mp: 114–116 °C. ^{1}H-NMR (400 MHz, $CDCl_3$): δ 9.06 (s, 1H), 8.34 (br s, 1H), 7.74 (d, J = 9.2 Hz, 1H), 7.47–7.42 (m, 2H), 7.00 (t, J = 8.4 Hz, 1H), 5.24 (d, J = 6.1 Hz, 2H). ^{13}C-NMR (101 MHz, $CDCl_3$): δ 163.1, 157.6 (d, J = 251.5 Hz), 149.8, 145.2, 131.9 (d, J = 8.7 Hz), 130.6 (d, J = 5.8 Hz), 129.1 (d, J = 4.2 Hz), 125.8 (d, J = 22.6 Hz), 124.1 (q, J = 6.3 Hz), 124.0, 121.4, 119.0 (q, J = 34.8 Hz), 116.9, 115.5 (d, J = 23.2 Hz), 33.5. IR (neat): $\tilde{\nu}$ = 3039, 2924, 2854, 1718, 1554, 1180, 1126, 810, 740 cm^{-1}. MS (ESI): m/z 407 [M+

H]$^+$. HRMS (ESI) *m/z* (M + Na)$^+$ calcd for $C_{15}H_8Cl_2F_4N_4ONa$ 428.9909, found 428.9894.

2,6-Difluoro-4-methoxy-N-((6-(trifluoromethyl)-[1,2,4]triazolo [4,3-a]pyridin-3-yl)methyl)benzamide, (16)

PE/EtOAc 2:8. White solid. Yield 68%; mp: 215–216 °C, dec. ^{1}H-NMR (400 MHz, $(CD_3)_2CO$): δ 9.18 (s, 1H), 8.38 (br s, 1H), 7.93 (d, *J* = 9.3 Hz, 1H), 7.60 (d, *J* = 9.6 Hz, 1H), 6.65 (d, *J* = 10.4 Hz, 2H), 5.26 (s, 2H), 3.83 (s, 3H). ^{13}C-NMR (101 MHz, DMSO-d_6): δ 162.2 (t, *J* = 14.0 Hz), 161.0, 160.2 (dd, J_s = 234.5 Hz, 11.0 Hz), 149.5, 146.5, 125.5 (q, *J* = 6.1 Hz), 123.8 (q, *J* = 269.5 Hz), 123.6, 117.3, 116.3 (q, *J* = 33.2 Hz), 107.4 (t, *J* = 22.5 Hz), 98.9 (d, *J* = 24.9 Hz), 56.8, 33.8. IR (neat): $\tilde{\nu}$ = 3309, 2923, 1640, 1494, 1217, 1040, 1019, 819, 782 cm^{-1}. MS (ESI): *m/z* 409 [M + Na]$^+$. HRMS (ESI) *m/z* (M + H)$^+$ calcd for $C_{16}H_{12}F_5N_4O_2$ 387.0875, found 387.0865.

4-Methoxy-2,6-dimethyl-N-((6-(trifluoromethyl)-[1,2,4]triazolo [4,3-a]pyridin-3-yl)methyl)benzamide, (17)

PE/EtOAc 4:6. White solid. Yield 47%; mp: 133–135 °C. ^{1}H-NMR (400 MHz, DMSO-d_6): δ 9.25 (s, 1H), 8.99 (br s, 1H), 7.99 (d, *J* = 9.6 Hz, 1H), 7.64 (d, *J* = 9.6 Hz, 1H), 6.60 (s, 2H), 5.06 (d, *J* = 5.9 Hz, 2H), 3.71 (s, 3H), 2.10 (s, 6H). ^{13}C-NMR (101 MHz, DMSO-d_6): δ 170.4, 159.4, 149.4, 147.1, 135.9, 130.8, 125.8 (q, *J* = 6.0 Hz), 123.9 (q, *J* = 272 Hz), 122.5, 117.3, 116.2 (q, *J* = 33.5 Hz), 113.0, 55.5, 33.4, 19.4. IR (neat): $\tilde{\nu}$ = 3420, 3057, 2923, 1633, 1317, 1122, 819, 697 cm^{-1}. MS (ESI): *m/z* 379 [M + H]$^+$. HRMS (ESI) *m/z* (M + H)$^+$ calcd for $C_{18}H_{18}F_3N_4O_2$ 379.1376, found 379.1368.

4,4′-Difluoro-N-((6-(trifluoromethyl)-[1,2,4]triazolo[4,3-a] pyridin-3-yl)methyl)-[1,1′-biphenyl]-3-carboxamide, (18)

PE/EtOAc 4:6. White solid. Yield 62%; mp: 177–178 °C. ^{1}H-NMR (400 MHz, $CDCl_3$): δ 9.19 (s, 1H), 8.26 (dd, J_s = 7.3, 2.6 Hz, 1H), 7.85 (d, *J* = 9.6 Hz, 2H), 7.67–7.64 (m, 1H), 7.55–7.52 (m, 2H), 7.43 (d, *J* = 11.1 Hz, 1H), 7.20–7.11 (m, 3H), 5.29 (d, *J* = 5.8 Hz, 2H). ^{13}C-NMR (101 MHz, $CDCl_3$): δ 164.3, 162.8 (d, *J* = 247.7 Hz), 160.1 (d, *J* = 249.3 Hz), 149.9, 145.9, 137.4 (d, *J* = 3.2 Hz), 135.1 (d, *J* = 3.1 Hz), 132.3 (d, *J* = 9.4 Hz), 130.3, 128.7,124.0 (q, *J* = 5.9 Hz), 123.6 (d, *J* = 2.1 Hz), 122.8 (q, *J* = 270.0 Hz), 120.1 (d, *J* = 11.7 Hz), 118.9 (d, *J* = 6.3 Hz), 118.7 (q, *J* = 34.2 Hz), 116.7 (d, *J* = 25.1 Hz), 115.9 (d, *J* = 21.7 Hz), 33.7. IR (neat): $\tilde{\nu}$ = 3221, 3056, 2925, 1717, 1646, 1488, 1223, 1143, 813, 744 cm^{-1}. MS (ESI): *m/z* 433 [M + H]$^+$. HRMS (ESI) *m/z* (M + H)$^+$ calcd for $C_{21}H_{14}F_5N_4O$ 433.1082, found 433.1074.

4′-Cyano-4-fluoro-N-((6-(trifluoromethyl)-[1,2,4]triazolo[4,3-a] pyridin-3-yl)methyl)-[1,1′-biphenyl]-3-carboxamide, (19)

PE/EtOAc 3:7. White solid. Yield 63%; mp: 213–215 °C. ^{1}H-NMR (400 MHz, DMSO-d_6): δ 9.30 (br s, 1H), 9.24 (s, 1H), 7.99 (d, *J* = 9.7 Hz, 1H), 7.95–7.88 (m, 7H), 7.63 (d, *J* = 9.7 Hz, 1H), 7.46–7.42 (m, 1H), 5.12 (d, *J* = 5.6 Hz, 2H). ^{13}C-NMR (101 MHz, DMSO-d_6): δ 164.6, 160.0 (d, *J* = 252.9 Hz), 149.5, 146.7, 143.3, 135.1 (d, *J* = 3.6 Hz), 133.4, 131.9 (d, *J* = 8.8 Hz), 129.1 (d, *J* = 3.3 Hz), 128.1, 125.7 (q, *J* = 6.0 Hz), 124.2 (d, *J* = 14.5 Hz), 123.6 (d, *J* = 3.0 Hz), 123.4 (q, *J* = 272.6 Hz), 119.2, 117.7 (d, *J* = 22.6 Hz), 117.3, 116.3 (d, *J* = 33.5 Hz), 110.9, 34.0. IR (neat): $\tilde{\nu}$ = 3202, 3039, 2924, 2225, 1650, 1487, 1148, 821, 747 cm^{-1}. MS (ESI): *m/z* 440 [M + H]$^+$. HRMS (ESI) *m/z* (M + H)$^+$ calcd for $C_{22}H_{14}F_4N_5O$ 440.1129, found 440.1122.

4-Fluoro-2′-methyl-N-((6-(trifluoromethyl)-[1,2,4]triazolo [4,3-a]pyridin-3-yl)methyl)-[1,1′-biphenyl]-3-carboxamide, (20)

PE/EtOAc 7:3. Colourless oil. Yield 65%. ^{1}H-NMR (400 MHz, $(CD_3)_2CO$): δ 9.33 (s, 1H), 8.50 (br s, 1H),7.90 (d, *J* = 9.7 Hz, 1H), 7.83 (dd, J_s = 7.1, 2.4 Hz, 1 H), 7.56 (dd, J_s = 9.5, 1.6 Hz, 1 H), 7.54–7.52 (m, 1H), 7.34–7.29 (m, 4H), 7.28–7.24 (m, 1H), 5.30 (d, *J* = 5.9 Hz, 2H), 2.23 (s, 3H). ^{13}C-NMR (101 MHz, $(CD_3)_2CO$): δ 164.3, 159.3 (d, *J* = 247.9 Hz), 149.5, 146.3, 139.9, 138.5 (d, *J* = 14.5 Hz), 135.1, 131.3 (d, *J* = 2.7 Hz), 130.4, 129.5, 127.8, 126.0, 125.1 (q, *J* = 6.2 Hz), 123.7 (q, *J* = 269.1 Hz), 122.6 (2 C), 121.8 (d, *J* = 13.2 Hz), 116.9, 116.7 (q, *J* = 33.8 Hz), 116.0 (d, *J* = 23.7 Hz), 33.8, 19.5. IR (neat): $\tilde{\nu}$ = 3194, 2924, 2854, 1652, 1524, 1316, 1125, 819, 732 cm^{-1}. MS (ESI): *m/z* 429 [M + H]$^+$. HRMS (ESI) *m/z* (M + H)$^+$ calcd for $C_{22}H_{17}F_4N_4O$ 429.1333, found 429.1325.

4-Fluoro-4′-methoxy-N-((6-(trifluoromethyl)-[1,2,4]triazolo [4,3-a]pyridin-3-yl)methyl)-[1,1′-biphenyl]-3-carboxamide, (21)

PE/EtOAc 3:7. White solid. Yield 60%; mp: 215–217 °C. ^{1}H-NMR (400 MHz, DMSO-d_6): δ 9.25–9.22 (m, 2H), 7.99 (d, *J* = 9.6 Hz, 1H), 7.81–7.74 (m, 2H), 7.64–7.58 (m, 4H), 7.34 (t, *J* = 8.6 Hz, 1H), 7.02 (d, *J* = 8.6 Hz, 1H), 5.11 (d, *J* = 5.7 Hz, 2H), 3.79 (s, 3H). ^{13}C-NMR (101 MHz, DMSO-d_6): δ 164.9, 159.6, 158.9 (d, *J* = 251.4 Hz), 149.5, 146.7, 136.7 (d, *J* = 3.2 Hz), 131.2, 130.8 (d, *J* = 8.5 Hz), 128.3, 127.9 (d, *J* = 2.8 Hz), 125.7 (q, *J* = 6.0 Hz), 123.9 (2 C), 123.6 (d, *J* = 2.9 Hz), 117.3, 117.2 (d, *J* = 22.5 Hz), 116.3 (q, *J* = 34.0 Hz), 114.9, 55.7, 34.0. IR (neat): $\tilde{\nu}$ = 3334, 1643, 1612, 1546, 1487, 1222, 1178, 815, 730 cm^{-1}. MS (ESI): *m/z* 445 [M + H]$^+$. HRMS (ESI) *m/z* (M + H)$^+$ calcd for $C_{22}H_{17}F_4N_4O_2$ 445.1282, found 445.1274.

4′-Methyl-N-((6-(trifluoromethyl)-[1,2,4]triazolo[4,3-a]pyridin-3-yl)methyl)-[1,1′-biphenyl]-3-carboxamide, (22)

PE/EtOAc 4:6. Yellow solid. Yield 42%; mp: 195–197 °C. ^{1}H-NMR (400 MHz, $CDCl_3$): δ 9.33 (s, 1H), 8.77 (br s, 1H), 8.23 (s, 1H), 7.95 (d, *J* = 7.8 Hz, 1H), 7.71 (d, *J* = 7.9 Hz, 2H), 7.50–7.46 (m, 3H), 7.39 (d, *J* = 9.6 Hz, 1H) 7.20 (d, *J* = 7.9 Hz, 2H), 5.25 (d, *J* = 5.9 Hz, 2H), 2.38 (s, 3H). ^{13}C-NMR (101 MHz, $CDCl_3$): δ 168.5, 149.8, 146.8, 141.6, 137.6, 137.1, 133.6, 130.5, 129.5, 129.1, 127.0, 126.1, 126.0, 124.6 (q, *J* = 6.1 Hz), 123.8, 122.9 (q, *J* = 272.8 Hz), 118.7 (q, *J* = 34.7 Hz), 116.9, 33.6, 21.1. IR (neat): $\tilde{\nu}$ = 3040, 2928, 1655, 1545, 1317, 1172, 1126, 787 cm^{-1}. MS (ESI): *m/z* 411 [M + H]$^+$. HRMS (ESI) *m/z* (M + H)$^+$ calcd for $C_{22}H_{18}F_3N_4O$ 411.1427, found 411.1424.

2-Fluoro-5-iodo-N-((6-(trifluoromethyl)-[1,2,4]triazolo[4,3-a] pyridin-3-yl)methyl)benzamide, (23)

PE/EtOAc 4:6. Yellow solid. Yield 70%; mp 157–159 °C. ^{1}H-NMR (400 MHz, CD_3OD): δ 9.22 (s, 1H), 8.05 (dd, J_s = 6.7 Hz, 2.4 Hz, 1H), 7.93 (d, *J* = 9.7 Hz, 1H), 7.87–7.83 (m, 1H), 7.66 (d, *J* = 9.8 Hz, 1H), 7.03 (dd, J_s = 10.6 Hz, 8.7 Hz, 1H), 5.18 (s, 2H). ^{13}C-NMR (101 MHz, CD_3OD): δ 164.4, 159.9 (d, *J* = 250.0 Hz), 149.7, 146.3, 141.9 (d, *J* = 8.7 Hz), 138.8 (d, *J* = 2.2 Hz), 124.6 (q, *J* = 6.2 Hz), 124.3 (d, *J* = 18.2 Hz), 124.1, 123.1 (q, *J* = 245.0 Hz), 118.2 (d, *J* = 24.0 Hz), 118.1 (q, *J* = 34 Hz), 116.2, 86.5, 33.4. IR (neat): $\tilde{\nu}$ = 3337, 3052, 2932, 1642, 1547, 1317, 1175, 1122, 811, 640 cm^{-1}. MS (ESI): *m/z* 487 [M + Na]$^+$.

General procedure for the synthesis of compounds 24–25

In a Schlenk tube, intermediate **23** (100 mg, 0.21 mmol) was solubilized in dry DMF (0.5 mL) and dry EtOH (0.5 mL). Then, boronic acid (0.32 mmol, 1.5 eq), $Pd(OAc)_2$ (1.5 mg, 0.0022 mmol), K_2CO_3 (59.5 mg, 0.43 mmol) were added and two freeze-pump-

thaw cycles were performed at −78 °C. The reaction mixture was stirred at 80 °C overnight. The mixture was filtered over a pad of celite and rinsed with ethanol and then the volatile was removed. Purification by silica gel column chromatography afforded compounds **24**–**25**.

4-Fluoro-3′,4′-dimethyl-N-((6-(trifluoromethyl)-[1,2,4]triazolo [4,3-a]pyridin-3-yl)methyl)-[1,1′-biphenyl]-3-carboxamide, (24)

PE/EtOAc 6:4. Amorphous white solid. Yield 48%. ^{1}H-NMR (400 MHz, CD_3OD): δ 9.25 (s, 1H), 7.94–7.89 (m, 2H), 7.73–7.70 (m, 1H), 7.64 (d, J=8.0 Hz, 1H), 7.34 (s, 1H), 7.29–7.21 (m, 2H), 7.16 (d, J=7.8 Hz, 1H), 5.21 (s, 2H), 2.30 (s, 3H), 2.28 (s, 3H). ^{13}C-NMR (101 MHz, CD_3OD): δ 166.1, 159.3 (d, J=248.6 Hz), 137.8, 136.9, 136.4, 136.0, 131.2 (d, J=8.7 Hz), 128.7 (q, J=225.3 Hz), 128.1, 128.0, 124.6 (q, J=6 Hz), 124.1, 123.8, 122.4 (d, J=7.3 Hz), 121.9 (d, J=14.1 Hz), 118.0 (q, J=34.0 Hz), 116.3 (d, J=23.1 Hz), 116.2, 115.3, 33.4, 18.5, 18.0. IR (neat): $\tilde{\nu}$=2961, 2924, 2854, 1654, 1316, 1259, 1095, 1017, 795 cm^{-1}. MS (ESI): *m/z* 443 $[M+H]^+$. HRMS (ESI) *m/z* $(M+H)^+$ calcd for $C_{23}H_{19}F_4N_4O$ 443.1490, found 443.1466.

4-Fluoro-3′,4′-dimethoxy-N-((6-(trifluoromethyl)-[1,2,4]triazolo [4,3-a]pyridin-3-yl)methyl)-[1,1′-biphenyl]-3-carboxamide, (25)

PE/EtOAc 5:5. Amorphous yellow solid. Yield 37%. ^{1}H-NMR (400 MHz, CD_3OD): δ 9.25 (s, 1H), 7.95–7.90 (m, 2H), 7.76–7.72 (m, 1H), 7.65 (d, J=9.7 Hz, 1H), 7.24 (dd, J_s=10.6, 8.7 Hz, 1H), 7.17–7.14 (m, 2H), 7.01 (d, J=8.2 Hz, 1H), 5.20 (s, 2H), 3.89 (s, 3H), 3.86 (s, 3H). ^{13}C-NMR (101 MHz, CD_3OD): δ 166.1, 159.1 (d, J=249.1 Hz), 149.5 (2 C), 149.2, 137.6, 132.0, 131.1 (d, J=8.7 Hz), 128.4, 128.0, 127.7, 124.6 (q, J=6.5 Hz), 124.1 (d, J=2.2 Hz), 122.0 (d, J=16.6 Hz), 118.1 (q, J=34.0 Hz), 117.7 (q, J=295.5 Hz), 116.3 (d, J=23.0 Hz), 115.3, 112.0, 110.5, 55.2, 55.1, 33.5. IR (neat): $\tilde{\nu}$=2920, 2850, 1654, 1488, 1464, 1258, 1096, 1021, 802, 765 cm^{-1}. MS (ESI): *m/z* 475 $[M+H]^+$. HRMS (ESI) *m/z* $(M+Na)^+$ calcd for $C_{23}H_{18}F_4N_4ONa$ 497.1213, found 497.1194.

General procedure for the synthesis of compounds 30–31

Amine **29** (100 mg, 0.34 mmol, 1 eq) was solubilized in dry CH_2Cl_2 (2.5 mL) under nitrogen. TEA (104 μL, 0.75 mmol, 2.2 eq), HOBt (55.4 mg, 0.41 mmol, 1.2 eq), EDCI (78.6 mg, 0.41 mmol, 1.2 eq) and carboxylic acid (0.41 mmol, 1.2 eq) were added in order. The reaction was stirred at room temperature overnight, then the volatile was removed. The crude material was diluted with EtOAc and washed with water (3x). The organic layer was dried over sodium sulfate and evaporated. Purification by silica gel column chromatography afforded compounds **30**–**31**.

N-((6-Chloro-[1,2,4]triazolo[4,3-a]pyridin-3-yl)methyl)-1H-indazole-7-carboxamide, (30)

EtOAc. White solid. Yield 42%; mp 268–270 °C, dec. ^{1}H-NMR (400 MHz, DMSO-d_6): δ 13.14 (br s, 1H), 9.42 (br s, 1H), 8.92 (s, 1H), 8.17 (s, 1H), 7.99 (d, J=7.8 Hz, 1H), 7.92, (d, J=7.2 Hz, 1H), 7.84 (d, J=9.7 Hz, 1H), 7.44 (dd, J_s=9.7, 1.8 Hz, 1H), 7.20 (t, J=7.6 Hz, 1H), 5.09 (d, J=3.1 Hz, 2H). ^{13}C-NMR (101 MHz, DMSO-d_6): δ 166.8, 148.5, 145.6, 138.1, 134.2, 129.3, 125.5, 125.4, 124.9, 122.9, 121.0, 120.2, 116.7 (2 C), 33.8. IR (neat): $\tilde{\nu}$=3238, 3052, 1641, 1566, 1315, 1288, 925, 826, 736 cm^{-1}. MS (ESI): *m/z* 327 $[M+H]^+$. HRMS (ESI) *m/z* $(M+H)^+$ calcd for $C_{15}H_{12}ClN_6O$ 327.0756, found 327.0749.

N-((6-Chloro-[1,2,4]triazolo[4,3-a]pyridin-3-yl)methyl)-2-fluoro-5-iodobenzamide, (31)

PE/EtOAc 3:7. Amorphous white solid. Yield 40%. ^{1}H-NMR (400 MHz, $CDCl_3$): δ 8.83 (s, 1H), 8.06 (dd, J_s=6.6, 2.3 Hz, 1H), 7.89–7.84 (m, 1H), 7.78 (dd, Js=9.8, 1.0 Hz,1H), 7.50 (dd, J_s=9.8, 1.8 Hz, 1H), 7.04 (dd, J_s=10.5, 8.6 Hz, 1H), 5.11 (s, 2H). ^{13}C-NMR (101 MHz, $CDCl_3$): δ 165.8, 159.2, 149.9, 146.3, 142.0, 137.8, 129.5, 126.6, 124.0, 123.2, 117.1, 116.2, 86.9, 33.6. IR (neat): $\tilde{\nu}$=3242, 3052, 2917, 1644, 1543, 1316, 1175, 1120, 813, 642 cm^{-1}. MS (ESI): *m/z* 432 $[M+H]^+$.

Synthesis of compound N-((6-Chloro-[1,2,4]triazolo[4,3-a] pyridin-3-yl)methyl)-4-fluoro-3′,4′-dimethoxy-[1,1′-biphenyl]-3-carboxamide, (32)

In a Schlenk tube, intermediate **31** (50 mg, 0.12 mmol) was solubilized in dry DMF (0.5 mL) and dry EtOH (0.5 mL). Then, (3,4-dimethoxyphenyl)boronic acid (31.7 mg, 0.17 mmol), $Pd(OAc)_2$ (0.8 mg, 0.0016 mmol), K_2CO_3 (32.1 mg, 0.23 mmol) were added, and two freeze-pump-thaw cycles were performed at −78 °C. The reaction mixture was stirred at 80 °C overnight. The mixture was filtered over a pad of celite and rinsed with methanol and then the volatile was removed. The crude material was purified by column chromatography using PE/EtOAc 3:7. Amorphous white solid. Yield 70%. ^{1}H-NMR (400 MHz, CD_3OD): δ 8.83 (s, 1H), 7.92 (dd, J_s=6.9, 2.5 Hz, 1H), 7.73–7.71 (m, 2H), 7.43 (d, J=9.7 Hz, 1H), 7.21 (dd, J_s=9.6, 8.7 Hz, 1H), 7.13–7.10 (m, 2H), 6.96 (d, J=8.3 Hz, 1H), 5.12 (s, 2H), 3.87 (s, 3H), 3.33 (s, 3H). ^{13}C-NMR (101 MHz, CD_3OD): δ 165.9, 159.2 (d, J=248.5 Hz), 149.5 (2 C), 149.2 (2 C), 137.7 (d, J=3.5 Hz), 132.0, 131.1 (d, J=8.7 Hz), 130.0, 128.0, 122.4, 122.2, 121.9 (d, J=13.7 Hz), 119.2, 116.2 (d, J=23.1 Hz), 115.5, 112.0, 110.5, 55.2, 55.1, 33.4. IR (neat): $\tilde{\nu}$=2957, 2922, 2853, 1652, 1487, 1248, 1021, 798, 654 cm^{-1}. MS (ESI): *m/z* 464 $[M+Na]^+$. HRMS (ESI) *m/z* $(M+H)^+$ calcd for $C_{22}H_{19}ClFN_4O_3$ 441.1124, found 441.1117.

General procedure for the synthesis of compounds 37–40, 42, 44

The corresponding amine (**36**, **41**, **43**) (0.32 mmol) was solubilized in dry CH_2Cl_2 (2.5 mL) under nitrogen. TEA (97 μL, 0.70 mmol), HOBt (51.3 mg, 0.38 mmol), EDCI (72.8 mg, 0.38 mmol) and carboxylic acid (0.32 mmol) were added in order. The reaction was stirred at room temperature overnight. The volatile was removed under vacuo, then diluted with EtOAc and washed with water (3x). The organic layer was dried over sodium sulfate and evaporated. Purification by silica gel column chromatography afforded compounds **37**–**40**, **42**, **44**.

N-([1,2,4]Triazolo[4,3-a]quinolin-1-ylmethyl)-1H-indazole-7-carboxamide, (37)

EtOAc/MeOH 98:2. White solid. Yield 69%; mp: 251.5–253 °C, dec. ^{1}H-NMR (400 MHz, DMSO-d_6): δ 9.36 (br s, 1H), 8.24 (d, J=8.6 Hz, 1H), 8.17 (br s, 1H), 8.03 (d, J=7.6 Hz, 1H), 7.97 (d, J=7.9 Hz, 1H), 7.87 (d, J=8.1 Hz, 1H), 7.83 (d, J=9.6 Hz, 1H), 7.74 (s, 1H), 7.72–7.70 (m, 2H), 7.59 (t, J=7.8 Hz, 2H), 5.43 (d, J=4.8 Hz, 2H). ^{13}C-NMR (101 MHz, DMSO-d_6): δ 167.4, 150.2, 146.9, 132.2, 132.0, 130.4, 130.3, 129.8, 129.1 (2 C), 126.7, 126.4, 124.5, 124.3, 119.2, 117.5, 115.0, 110.5, 38.6. IR (neat): $\tilde{\nu}$=3268, 3082, 2923, 1638, 1592, 1558, 1314, 1028, 800, 744 cm^{-1}. MS (ESI): *m/z* 343 $[M+H]^+$. HRMS (ESI) *m/z* $(M+H)^+$ calcd for $C_{19}H_{15}N_6O$ 343.1302, found 343.1293.

N-([1,2,4]Triazolo[4,3-a]quinolin-1-ylmethyl)-3-bromo-4-hydroxybenzamide, (38)

EtOAc/MeOH 9:1. White solid. Yield 61%; mp: 204–206 °C, dec. ^{1}H-NMR (400 MHz, DMSO-d_6): δ 9.02 (br s, 1H), 8.13 (d, J=8.5 Hz, 1H), 8.04–8.02 (m, 2H), 7.81 (t, J=7.5 Hz, 1H), 7.77–7.76 (m, 1H), 7.73 (s, 1H), 7.67 (d, J=7.5 Hz, 1H), 7.59 (t, J=7.5 Hz, 1H), 7.52 (d, J=8.1 Hz, 1H), 5.27 (s, 2H). ^{13}C-NMR (101 MHz, DMSO-d_6): δ 165.8, 158.0, 150.2, 146.8, 132.7, 130.2, 129.8, 128.9, 128.1, 126.4, 125.9, 124.5, 123.7, 118.9, 117.4, 116.4, 115.0, 38.2. IR (neat): $\tilde{\nu}$=3329, 2918, 2849, 1621, 1510, 1426, 1280, 811, 752, 680 cm^{-1}. MS (ESI): *m/z* 397 [M+H]$^+$. HRMS (ESI) *m/z* (M+H)$^+$ calcd for $C_{18}H_{14}BrN_4O_2$ 397.0295, found 397.0286.

N-([1,2,4]Triazolo[4,3-a]quinolin-1-ylmethyl)-4-methoxy-2,6-dimethylbenzamide, (39)

PE/EtOAc 3:7. White solid. Yield 89%; mp: 219–220 °C. ^{1}H-NMR (400 MHz, DMSO-d_6): δ 8.90 (br s, 1H), 8.28 (d, J=8.5 Hz, 1H), 8.04 (d, J=9.4 Hz, 1H), 7.82–7.7.73 (m, 2H), 7.69 (d, J=9.6 Hz, 1H), 7.64 (t, J=8.1 Hz, 1H), 6.59 (s, 2H), 5.29 (d, J=4.9 Hz, 2H), 3.66 (s, 3H), 2.26 (s, 6H). ^{13}C-NMR (100 MHz, DMSO-d_6): δ 170.1, 159.3, 150.0, 146.7, 136.2, 131.9, 131.0, 130.3, 130.1, 129.8, 126.7, 124.5, 117.7, 115.0, 112.9, 55.4, 37.8, 19.8. IR (neat): $\tilde{\nu}$=3235, 2920, 1671, 1527, 1320, 1284, 1167, 806, 749, 731 cm^{-1}. MS (ESI): *m/z* 361 [M+H]$^+$. HRMS (ESI) *m/z* (M+H)$^+$ calcd for $C_{21}H_{21}N_4O_2$ 361.1659, found 361.1649.

N-([1,2,4]triazolo[4,3-a]quinolin-1-ylmethyl)-4-fluoro-4′-methoxy-[1,1′-biphenyl]-3-carboxamide, (40)

PE/EtOAc 1:9. White solid. Yield 75%; mp: 195–197 °C, dec. ^{1}H-NMR (400 MHz, $CDCl_3$): δ 8.33 (dd, J_s=7.2, 2.6 Hz, 1H), 8.20 (d, J=8.5 Hz, 1 H), 7.86 (d, J=7.9 Hz, 1H), 7.76 (t, J=7.1 Hz, 1H), 7.70–7.65 (m, 2H), 7.62–7.59 (m, 2H), 7.55 (d, J=8.8 Hz, 2H), 7.20 (dd, J_s=11.3, 8.6 Hz, 1H), 7.01 (d, J=8.8 Hz, 2H), 5.56 (s, 2H), 3.86 (s, 3H). ^{13}C-NMR (101 MHz, $CDCl_3$): δ 163.8, 159.9 (d, J=247.7 Hz), 159.5, 150.7, 145.6, 137.7 (d, J=3.0 Hz), 131.7, 131.6 (d, J=10.8 Hz), 130.0 (d, J=2.9 Hz), 129.7, 129.6, 129.4, 128.1, 126.5, 124.5, 120.5 (d, J=11.6 Hz), 116.7, 116.5 (2 C), 114.9, 114.4 (2 C), 55.4, 39.5. IR (neat): $\tilde{\nu}$=3279, 2916, 2848, 1626, 1483, 1247, 1216, 813, 752 cm^{-1}. MS (ESI): *m/z* 427 [M+H]$^+$. HRMS (ESI) *m/z* (M+H)$^+$ calcd for $C_{25}H_{20}FN_4O_2$ 427.1565, found 427.1546.

N-([1,2,4]Triazolo[4,3-a]pyridin-3-ylmethyl)-1H-indazole-7-carboxamide, (42)

EtOAc/MeOH 9:1. Pale yellow solid. Yield 65%; mp: 254–256 °C, dec. ^{1}H-NMR (400 MHz, DMSO-d_6): δ 13.12 (br s, 1H), 9.40 (br s, 1H), 8.65 (d, J=7.0 Hz, 1H), 8.16 (s, 1H), 7.98 (d, J=7.9 Hz, 1H), 7.93 (d, J=7.3 Hz, 1H), 7.77 (d, J=9.2 Hz, 1H), 7.39 (t, J=6.5 Hz, 1H), 7.19 (t, J=7.6 Hz, 1H), 7.02 (t, J=6.7 Hz, 1H), 5.13 (s, 2H). ^{13}C-NMR (100 MHz, DMSO-d_6): δ 166.8, 150.0, 145.0, 138.2, 134.2, 128.1, 125.5, 125.3, 124.8, 120.1, 116.8, 115.7, 114.0 (2 C), 33.9. IR (neat): $\tilde{\nu}$=3320, 3040, 2923, 1636, 1539, 1333, 1301, 763, 726 cm^{-1}. MS (ESI): *m/z* 315 [M+Na]$^+$. HRMS (ESI) *m/z* (M+H)$^+$ calcd for $C_{15}H_{13}N_6O$ 293.1145, found 293.1137.

N-(Naphthalen-1-ylmethyl)-1H-indazole-7-carboxamide, (44)

EtOAc/MeOH 9:1. Dark yellow solid. Yield 90%; mp: 188–190 °C, dec. ^{1}H-NMR (400 MHz, DMSO-d_6): δ 13.09 (br s, 1H), 9.22 (br s, 1H), 8.26 (d, J=8.1 Hz, 1H), 8.16 (s, 1H), 8.00–7.96 (m, 3H), 7.87 (d, J=8.0 Hz, 1H), 7.61–7.53 (m, 3H), 7.49 (t, J=7.8 Hz, 1H), 7.20 (t, J=7.6 Hz, 1H), 5.06 (d, J=5.7 Hz, 2H). ^{13}C-NMR (101 MHz, DMSO-d_6): δ 166.3, 138.4, 135.1, 134.0, 133.8, 131.4, 129.0, 128.0, 126.7, 126.2, 125.9 (2 C), 125.2, 124.9, 123.9 (2 C), 120.1, 117.4, 41.0. IR (neat): $\tilde{\nu}$=3328, 2961, 2924, 1620, 1585, 1258, 1019, 789, 777 cm^{-1}. MS (ESI): *m/z* 300 [M–H]$^-$. HRMS (ESI) *m/z* (M+H)$^+$ calcd for $C_{19}H_{16}N_3O$ 302.1288, found 302.1282.

Molecular modelling

All molecular modelling studies were performed on a Tesla workstation equipped with two Intel Xeon X5650 2.67 GHz processors and Ubuntu 20.04.[56] Protein structures and 3D chemical structures were generated in PyMOL.[57]

Molecular docking

The X-ray structure of the 4-phenylimidazole-IDO1 complex was used (PDB id 2D0T).[36] Water molecules were removed, and all the hydrogen atoms and MMFF94 charges were added. Then, the complex was transferred into a fred_receptor and prepared for docking with FRED.[48,49] The interaction between the iron moiety of the heme group and the target molecule was used as a constraint: a chelator constraint is satisfied when a chelator on the ligand makes a metal-chelator interaction with the protein heavy atom. Docked conformations were scored using Chemgauss4. The energy of every water molecule in the apo state and in the presence of the ligands was evaluated with SZMAP/GAMEPLAN.[51]

Molecular dynamics (MD) simulation

The MD simulation was carried out using the Desmond simulation package of Schrödinger LLC.[47] The X-ray structure of the 4-phenylimidazole-IDO1 complex was used (PDB id 2D0T),[36] water molecules were removed, and all hydrogen atoms and charges were added. An orthorhombic box (10 Å×10 Å×10 Å) with periodic boundary conditions was created and 11,696 water molecules were added. The NPT ensemble with the temperature 300 K and a pressure 1 bar was applied in all runs. The simulation length was 100 ns, preceded by 1 ps of relaxation time in which only light atoms were allowed to move. The OPLS_2005 force field parameters were used in all simulations for protein, heme and ligand atoms.[58] The long-range electrostatic interactions were calculated using the particle mesh Ewald method.[59] The cut-off radius in Coulomb interactions was 9.0 Å. The water molecules were explicitly described using the simple point charge model.[60] The Martyna-Tuckerman-Klein chain coupling scheme[61] with a coupling constant of 2.0 ps for the pressure control and the Nosé-Hoover chain coupling scheme[62] for the temperature control were used. Nonbonded forces were calculated using an r-RESPA integrator where the short-range forces and the long-range forces were updated every 1 and 3 steps, respectively. The trajectory sampling was done at an interval of 1.0 ps. The behaviour and interactions between the ligands and protein were analysed using the Simulation Interaction Diagram tool implemented in Desmond MD package. The stability of MD simulation was monitored by looking on the RMSDs of the ligand and the protein atom positions in time.

rhIDO1 enzymatic assay

The effects of VS9 on the enzymatic activity of IDO1 were determined using the IDO1 inhibitor screening kit (BioVision Incorporate Milpitas CA, USA), according to manufacturer instructions. VS9 (10 μM) was added to complete assay reaction buffer and incubated for 45 min at 37 °C. The reaction was stopped by the

addition of 30% (w/v) CCl_3COOH. After heating at 50 °C for 15 min, the reaction mixture was centrifuged at 1500 g for 10 min. The supernatant was transferred into a well of a 96-well microplate and mixed (1:1 ratio) with of 2% (w/v) *p*-dimethylaminobenzaldehyde (Ehrlich's reagent) in acetic acid. The yellow pigment derived from kynurenine was measured at 490 nm using an Ultramark Microplate Imaging System (Bio-Rad). A positive inhibition control, included in the kit, was added. The results are expressed as mean ± SEM of three different experiments run in triplicate.

Heme detection

Free heme in solution was detected with a commercially available hemin detection kit (SigmaAldrich, Cat. MAK036). 1 μM holo-IDO1 in 100 mM potassium phosphate buffer (pH 7.2) plus 1 mM CHAPS was incubated with different concentrations of VS9 or 20 μM of epacadostat for 120 min at 37 °C. Samples were diluted 100-fold in the provided hemin assay buffer and the kit reagents added according to the manufacturer's specification. Absorbance at 570 nm was measured on a Tecan microplate reader. Values are reported relative to the untreated sample and are the mean of n = 3 ± SD.[19]

Cell culture

Human A375 cells were cultured in DMEM medium with high glucose (4.5 g/L), containing 10% heat inactivated fetal bovine serum (FBS), 2 mM L-glutamine 100 U/mL of penicillin and 10 μg/mL of streptomycin (GE Healthcare, Milan, Italy). P1.HTR cells, a highly transfectable clonal variant of mouse mastocytoma P815, were transfected by electroporation with a plasmid coding for human IDO1 (P1.IDO1) or TDO (P1.TDO).[63] The construct expressing human IDO1 was generated from the cDNA of peripheral blood mononuclear cells (PBMCs) stimulated with IFN-γ,[63] while the one expressing human TDO was bought (Sino Biological). Stable transfectant cell lines were obtained by puromycin selection. Both cell lines were cultured in Iscove's Modified Dulbecco's Medium (Gibco, Invitrogen CA, USA) supplemented with 10% FCS (Gibco, Invitrogen CA, USA), 1 mM glutamine (Gibco, Invitrogen CA, USA), and penicillin/streptomycin (Gibco, Invitrogen CA, USA).

MTT assay

Cell viability was measured by the 3-(4,5-dimethylthiazol-2-yl)-2,5-diphenyl-tetrazolium bromide (MTT) assay, as previously described.[32] A375 cells were seeded (0.5×10^5 cells/well) in 24-well plates and treated with each compound (10 μM) for 48 h at 37 °C in a 5% CO_2 humidified incubator. The percentage of cell viability was calculated as [100 (x-y)/(z-y)], where x, y, and z were the absorbance read in compound-treated, resting and compound-untreated cells, respectively. Results are expressed as mean ± SD of at least three experiments run in triplicate.

Cellular IDO1 inhibition

The enzymatic activity of IDO1 was evaluated by measuring the levels of L-Kyn into A375 cell media, as previously described.[31] A375 cells (0.5×10^5) were seeded in a 24-well culture plate (500 μL per well) and grown overnight. Serial dilutions (0.01–30 μM) of each compound in a total volume of 500 μL of the culture medium including human IFN-γ (500 U/mL final concentration) per well were added into wells containing the cells. All compounds were dissolved in DMSO (Sigma-Aldrich). The DMSO final concentration in the cell culture medium was always 0.1%. An equivalent amount of DMSO was added to drug-untreated controls. A preliminary progress curve was performed, and 48 h was set as the duration of the experiments to remain in the linear phase of the reaction. After 48 h of incubation, the cell medium was collected, deproteinized with 20% (v/v) aqueous CCl_3COOH, and centrifuged at 13200 rpm for 10 minutes, and the amounts of L-Kyn quantified by HPLC. 50 μL of supernatants were injected into a HPLC-VIS system (1525 Binary HPLC Pump with 2487 Dual λ absorbance detector, Waters), equipped with a C-18 Kinetex analytical column (5 μm particle size, 150 mm × 4.6 mm; Phenomenex, Torrance, CA, USA). The mobile phase (50 mM potassium dihydrogen phosphate, 10% v/v acetonitrile; pH 4.8) was delivered at a flow rate of 1 mL min^{-1} at room temperature, and the absorbance was measured at 330 nm. The amounts of L-Kyn in the A375 cell media were quantified on the basis of a calibration curve obtained using the same HPLC-VIS experimental setting. IC_{50} values were calculated from concentration-response curves obtained in at least three different experiments run in triplicate using GraphPad prism 9.1.0.

IDO1 and TDO selectivity assay

P1 transfected cells were used at a passage number not exceeding the 10^{th}. 1×10^5 P1.IDO1 or P1.TDO cells were incubated in a final volume of 400 μL with 10 μM of each compound for 16 h in a 48-well plate. The control was represented by cells incubated with an equivalent volume of DMSO, the vehicle in which compounds have been solubilized. After the incubation, supernatants of cell cultures were recovered and L-Kyn concentration was detected by HPLC-UV. Every cell assay was conducted in triplicate. Detection of L-Kyn concentrations was performed by using a PerkinElmer, series 200 HPLC instrument (MA, USA). A Kinetex C18 column (250 × 4.6 mm, 5 μm, 100 A; Phenomenex, USA), maintained at the temperature of 25 °C and pressure of 1800 PSI, was used. A sample volume of 300 μL was injected and eluted by a mobile phase containing 10 mM NaH_2PO_4 pH 3.0 (99%) and methanol (1%) (Sigma-Aldrich, MO, USA), with a flow rate of 1 mL/min. L-Kyn was detected at 360 nm by an UV detector. The software TURBOCHROM 4 was used for evaluating the concentration of L-Kyn in samples by means of a calibration curve. The detection limit of the analysis was 0.05 μM.

In vitro metabolic stability

Rat liver S9 (RLS9), (pooled male Sprague Dawley, protein concentration: 20 mg/mL) were purchased from Corning B.V. Life Sciences (Amsterdam, The Netherlands) and used throughout this study. The standard incubation mixture (250 μL final volume) was carried out in a 50 mM TRIS (tris[hydroxymethyl]aminomethane) buffer (pH 7.4) containing 3.3 mM $MgCl_2$, 1.3 mM β-NADP-Na_2, 3.3 mM glucose 6-phosphate, 0.4 Units/mL glucose 6-phosphate dehydrogenase (NADPH regenerating system), 5 μL of acetonitrile (1% of total volume), and the substrate compounds at a concentration of 5 μM. After pre-equilibration of the mixture, an appropriate volume of RLS9 suspension was added to give a final protein concentration of 1.5 mg/mL. The mixture was shaken for 60 min at 37 °C. Control incubations were carried out without the presence of RLS9 suspension or cofactors. Each incubation was stopped by addition of 250 μL ice-cold acetonitrile, vortexed and centrifuged at 13000 rpm for 10 min.

CYP inhibition: aminopyrine N-demethylase assay

CYP inhibitory potential of **25** and **38** was evaluated over aminopyrine *N*-demethylase activity by detecting the residual amount of formaldehyde after incubation of aminopyrine in rat liver microsomes (RLM). The assay was performed according to our previously

reported protocol and using ketoconazole as reference CYP inhibitor.[32]

Acknowledgements

M. S. is supported by Fondazione AIRC (Associazione Italiana per la Ricerca sul Cancro) fellowship for Abroad (Rif. 25278). T.P. and M.T.P. hold a grant from Ministero dell'Istruzione, dell'Università e della Ricerca (MIUR) (PRIN 2017 N° 2017WJZ9W9). Open Access Funding provided by Universita degli Studi del Piemonte Orientale Amedeo Avogadro within the CRUI-CARE Agreement.

Conflict of Interest

The authors declare no conflict of interest.

Keywords: Drug discovery · Indoleamine 2,3-dioxygenase-1 inhibitors · 1,2,4-triazole · Virtual screening · *in-silico* design

[1] D. Hanahan, R. A. Weinberg, *Cell* **2000**, *100*, 57–70.
[2] D. Hanahan, R. A. Weinberg, *Cell* **2011**, *144*, 646–674.
[3] Y. A. Fouad, C. Aanei, *Am. J. Cancer Res.* **2017**, *7*, 1016–1036.
[4] P. Sharma, S. Hu-Lieskovan, J. A. Wargo, A. Ribas, *Cell* **2017**, *168*, 707–723.
[5] R. W. Jenkins, D. A. Barbie, K. T. Flaherty, *Br. J. Cancer* **2018**, *118*, 9–16.
[6] N. P. Restifo, M. J. Smyth, A. Snyder, *Nat. Rev. Cancer* **2016**, *16*, 121–126.
[7] I. Melero, D. M. Berman, M. A. Aznar, A. J. Korman, J. L. P. Gracia, J. Haanen, *Nat. Rev. Cancer* **2015**, *15*, 457–472.
[8] S. J. Antonia, J. Larkin, P. A. Ascierto, *Clin. Cancer Res.* **2014**, *20*, 6258–6268.
[9] A. L. Mellor, H. Lemos, L. Huang, *Front. Immunol.* **2017**, *8*, 1360.
[10] J. Godin-Ethier, L.-A. Hanafi, C. A. Piccirillo, R. Lapointe, *Clin. Cancer Res.* **2011**, *17*, 6985–6991.
[11] A. Mondal, C. Smith, J. B. DuHadaway, E. Sutanto-Ward, G. C. Prendergast, A. Bravo-Nuevo, A. J. Muller, *EBioMedicine* **2016**, *14*, 74–82.
[12] F. Fallarino, U. Grohmann, S. You, B. C. McGrath, D. R. Cavener, C. Vacca, C. Orabona, R. Bianchi, M. L. Belladonna, C. Volpi, P. Santamaria, M. C. Fioretti, P. Puccetti, *J. Immunol.* **2006**, *176*, 6752–6761.
[13] D. H. Munn, M. D. Sharma, B. Baban, H. P. Harding, Y. Zhang, D. Ron, A. L. Mellor, *Immunity* **2005**, *22*, 633–642.
[14] M. T. Pallotta, C. Orabona, C. Volpi, C. Vacca, M. L. Belladonna, R. Bianchi, G. Servillo, C. Brunacci, M. Calvitti, S. Bicciato, E. M. C. Mazza, L. Boon, F. Grassi, M. C. Fioretti, F. Fallarino, P. Puccetti, U. Grohmann, *Nat. Immunol.* **2011**, *12*, 870–878.
[15] C. Orabona, M. T. Pallotta, U. Grohmann, *Mol. Med.* **2012**, *18*, 834–842.
[16] A. Iacono, A. Pompa, F. De Marchis, E. Panfili, F. A. Greco, A. Coletti, C. Orabona, C. Volpi, M. L. Belladonna, G. Mondanelli, E. Albini, C. Vacca, M. Gargaro, F. Fallarino, R. Bianchi, C. De Marcos Lousa, E. M. Mazza, S. Bicciato, E. Proietti, F. Milano, M. P. Martelli, I. M. Iamandii, M. Graupera Garcia-Mila, J. Llena Sopena, P. Hawkins, S. Suire, K. Okkenhaug, A. Stark, F. Grassi, M. Bellucci, P. Puccetti, L. Santambrogio, A. Macchiarulo, U. Grohmann, M. T. Pallotta, *EMBO Rep.* **2020**, *21*, DOI 10.15252/embr.201949756.
[17] Y. J. Lim, T. C. Foo, A. W. S. Yeung, X. Tu, Y. Ma, C. L. Hawkins, P. K. Witting, G. N. L. Jameson, A. C. Terentis, S. R. Thomas, *Biochemistry* **2019**, *58*, 974–986.
[18] M. T. Nelp, P. A. Kates, J. T. Hunt, J. A. Newitt, A. Balog, D. Maley, X. Zhu, L. Abell, A. Allentoff, R. Borzilleri, H. A. Lewis, Z. Lin, S. P. Seitz, C. Yan, J. T. Groves, *Proc. Natl. Acad. Sci. USA* **2018**, *115*, 3249–3254.
[19] R. F. Ortiz-Meoz, L. Wang, R. Matico, A. Rutkowska-Klute, M. De la Rosa, S. Bedard, R. Midgett, K. Strohmer, D. Thomson, C. Zhang, M. Mebrahtu, J. Guss, R. Totoritis, T. Consler, N. Campobasso, D. Taylor, T. Lewis, K. Weaver, M. Muelbaier, J. Seal, R. Dunham, W. Kazmierski, D. Favre, G. Bergamini, L. Shewchuk, A. Rendina, G. Zhang, *ChemBioChem* **2021**, *22*, 516–522.
[20] C. P. Stanley, G. J. Maghzal, A. Ayer, J. Talib, A. M. Giltrap, S. Shengule, K. Wolhuter, Y. Wang, P. Chadha, C. Suarna, O. Prysyazhna, J. Scotcher, L. L. Dunn, F. M. Prado, N. Nguyen, J. O. Odiba, J. B. Baell, J.-P. Stasch, Y. Yamamoto, P. Di Mascio, P. Eaton, R. J. Payne, R. Stocker, *Nature* **2019**, *566*, 548–552.
[21] X. Feng, D. Liao, D. Liu, A. Ping, Z. Li, J. Bian, *J. Med. Chem.* **2020**, *63*, 15115–15139.
[22] J. Le Naour, L. Galluzzi, L. Zitvogel, G. Kroemer, E. Vacchelli, *Oncoimmunology* **2020**, *9*, 1777625.
[23] U. F. Röhrig, A. Reynaud, S. R. Majjigapu, P. Vogel, F. Pojer, V. Zoete, *J. Med. Chem.* **2019**, *62*, 8784–8795.
[24] K. Garber, *Science* **2018**, *360*, 588–588.
[25] G. V. Long, R. Dummer, O. Hamid, T. F. Gajewski, C. Caglevic, S. Dalle, A. Arance, M. S. Carlino, J.-J. Grob, T. M. Kim, L. Demidov, C. Robert, J. Larkin, J. R. Anderson, J. Maleski, M. Jones, S. J. Diede, T. C. Mitchell, *Lancet Oncol.* **2019**, *20*, 1083–1097.
[26] B. J. Van den Eynde, N. van Baren, J.-F. Baurain, *Annu. Rev. Cancer Biol.* **2020**, *4*, 241–256.
[27] A. Balog, T. Lin, D. Maley, J. Gullo-Brown, E. H. Kandoussi, J. Zeng, J. T. Hunt, *Mol. Cancer Ther.* **2021**, *20*, 467–476.
[28] Bristol-Myers Squibb, *A Phase 3, Randomized, Study of Neoadjuvant Chemotherapy Alone Versus Neoadjuvant Chemotherapy Plus Nivolumab or Nivolumab and BMS-986205, Followed by Continued Post- Surgery Therapy With Nivolumab or Nivolumab and BMS-986205 in Participants With Muscle- Invasive Bladder Cancer*, Clinicaltrials.Gov, **2020**.
[29] S. Fallarini, A. Massarotti, A. Gesù, S. Giovarruscio, G. Coda Zabetta, R. Bergo, B. Giannelli, A. Brunco, G. Lombardi, G. Sorba, T. Pirali, *MedChemComm* **2016**, *7*, 409–419.
[30] A. Griglio, E. Torre, M. Serafini, A. Bianchi, R. Schmid, G. Coda Zabetta, A. Massarotti, G. Sorba, T. Pirali, S. Fallarini, *Bioorg. Med. Chem. Lett.* **2018**, *28*, 651–657.
[31] M. Serafini, E. Torre, S. Aprile, A. Massarotti, S. Fallarini, T. Pirali, *Molecules* **2019**, *24*, 1874.
[32] M. Serafini, E. Torre, S. Aprile, E. D. Grosso, A. Gesù, A. Griglio, G. Colombo, C. Travelli, S. Paiella, A. Adamo, E. Orecchini, A. Coletti, M. T. Pallotta, S. Ugel, A. Massarotti, T. Pirali, S. Fallarini, *J. Med. Chem.* **2020**, *63*, 3047–3065.
[33] T. Sterling, J. J. Irwin, *J. Chem. Inf. Model.* **2015**, *55*, 2324–2337.
[34] "eMolecules," can be found under https://www.emolecules.com/,**2021**.
[35] C. Tratrat, *Curr. Top. Med. Chem.* **2020**, *20*, 2235–2258.
[36] H. Sugimoto, S.-i. Oda, T. Otsuki, T. Hino, T. Yoshida, Y. Shiro, *Proc. Natl. Acad. Sci. USA* **2006**, *103*, 2611–2616.
[37] E. W. Yue, B. Douty, B. Wayland, M. Bower, X. Liu, L. Leffet, Q. Wang, K. J. Bowman, M. J. Hansbury, C. Liu, M. Wei, Y. Li, R. Wynn, T. C. Burn, H. K. Koblish, J. S. Fridman, B. Metcalf, P. A. Scherle, A. P. Combs, *J. Med. Chem.* **2009**, *52*, 7364–7367.
[38] S. Qian, T. He, W. Wang, Y. He, M. Zhang, L. Yang, G. Li, Z. Wang, *Bioorg. Med. Chem.* **2016**, *24*, 6194–6205.
[39] N. Pradhan, S. Paul, S. J. Deka, A. Roy, V. Trivedi, D. Manna, *ChemistrySelect* **2017**, *2*, 5511–5517.
[40] H. Tsujino, T. Uno, T. Yamashita, M. Katsuda, K. Takada, T. Saiki, S. Maeda, A. Takagi, S. Masuda, Y. Kawano, K. Meguro, S. Akai, *Bioorg. Med. Chem. Lett.* **2019**, *29*, 126607.
[41] U. F. Röhrig, S. R. Majjigapu, A. Grosdidier, S. Bron, V. Stroobant, L. Pilotte, D. Colau, P. Vogel, B. J. Van den Eynde, V. Zoete, O. Michielin, *J. Med. Chem.* **2012**, *55*, 5270–5290.
[42] D. Meininger, L. Zalameda, Y. Liu, L. P. Stepan, L. Borges, J. D. McCarter, C. L. Sutherland, *Biochim. Biophys. Acta* **2011**, *1814*, 1947–1954.
[43] U. F. Röhrig, S. R. Majjigapu, A. Reynaud, F. Pojer, N. Dilek, P. Reichenbach, K. Ascencao, M. Irving, G. Coukos, P. Vogel, O. Michielin, V. Zoete, *J. Med. Chem.* **2021**, *64*, 2205–2227.
[44] W. M. Kazmierski, B. Xia, J. Miller, M. De la Rosa, D. Favre, R. M. Dunham, Y. Washio, Z. Zhu, F. Wang, M. Mebrahtu, H. Deng, J. Basilla, L. Wang, G. Evindar, L. Fan, A. Olszewski, N. Prabhu, C. Davie, J. A. Messer, V. Samano, *J. Med. Chem.* **2020**, *63*, 3552–3562.
[45] M. M. Hamilton, F. Mseeh, T. J. McAfoos, P. G. Leonard, N. J. Reyna, A. L. Harris, A. Xu, M. Han, M. J. Soth, B. Czako, J. P. Theroff, P. K. Mandal, J. P. Burke, B. Virgin-Downey, A. Petrocchi, D. Pfaffinger, N. E. Rogers, C. A. Parker, S. S. Yu, Y. Jiang, S. Krapp, A. Lammens, G. Trevitt, M. R. Tremblay, K. Mikule, K. Wilcoxen, J. B. Cross, P. Jones, J. R. Marszalek, R. T. Lewis, *J. Med. Chem.* **2021**, *64*, 11302–11329.
[46] U. F. Röhrig, L. Awad, A. Grosdidier, P. Larrieu, V. Stroobant, D. Colau, V. Cerundolo, A. J. G. Simpson, P. Vogel, B. J. Van den Eynde, V. Zoete, O. Michielin, *J. Med. Chem.* **2010**, *53*, 1172–1189.

[47] Schrödinger Release 2020-1: Desmond Molecular Dynamics System; D. E. Shaw Research: New York, NY, 2019; Maestro-Desmond Interoperability Tools, Schrödinger, New York, NY, 2020.
[48] M. McGann, *J. Chem. Inf. Model.* **2011**, *51*, 578–596.
[49] FRED, version 3.0.0; OpenEye Scientific Software: Santa Fe, NM, http://www.eyesopen.com,**2020**.
[50] O. S. Software, "Cheminformatics Software | Molecular Modeling Software | OpenEye Scientific," can be found under https://www.eyesopen.com,**2020**.
[51] SZMAP, version 1.2.0, OpenEye Scientific Software, Inc., Santa Fe, NM, USA, www.eyesopen.com,**2013**.
[52] VIDA, version 4.4.0, OpenEye Scientific Software, Inc., Santa Fe, NM, USA, www.eyesopen.com,**2018**.
[53] A. A.-B. Badawy, *Int. J. Tryptophan Res.* **2017**, *10*, 117864691769193.
[54] D. Li, Y. Deng, A. Achab, I. Bharathan, B. A. Hopkins, W. Yu, H. Zhang, S. Sanyal, Q. Pu, H. Zhou, K. Liu, J. Lim, X. Fradera, C. A. Lesburg, A. Lammens, T. A. Martinot, R. D. Cohen, A. C. Doty, H. Ferguson, E. B. Nickbarg, M. Cheng, P. Spacciapoli, P. Geda, X. Song, N. Smotrov, P. Abeywickrema, C. Andrews, C. Chamberlin, O. Mabrouk, P. Curran, M. Richards, P. Saradjian, J. R. Miller, I. Knemeyer, K. M. Otte, S. Vincent, N. Sciammetta, A. Pasternak, D. J. Bennett, Y. Han, *ACS Med. Chem. Lett.* **2021**, *12*, 389–396.
[55] Q. Pu, H. Zhang, L. Guo, M. Cheng, A. C. Doty, H. Ferguson, X. Fradera, C. A. Lesburg, M. A. McGowan, J. R. Miller, P. Geda, X. Song, K. Otte, N. Sciammetta, N. Solban, W. Yu, D. L. Sloman, H. Zhou, A. Lammens, L. Neumann, D. J. Bennett, A. Pasternak, Y. Han, *ACS Med. Chem. Lett.* **2020**, *11*, 1548–1554.
[56] "Enterprise Open Source and Linux," can be found under https://ubuntu.com/,**2021**.
[57] The PyMOL Molecular Graphics System, version 2.4.1, Schrödinger LLC, **2021**.
[58] J. L. Banks, H. S. Beard, Y. Cao, A. E. Cho, W. Damm, R. Farid, A. K. Felts, T. A. Halgren, D. T. Mainz, J. R. Maple, R. Murphy, D. M. Philipp, M. P. Repasky, L. Y. Zhang, B. J. Berne, R. A. Friesner, E. Gallicchio, R. M. Levy, *J. Comput. Chem.* **2005**, *26*, 1752–1780.
[59] A. Y. Toukmaji, J. A. Board, *Comput. Phys. Commun.* **1996**, *95*, 73–92.
[60] J. Zielkiewicz, *J. Chem. Phys.* **2005**, *123*, 104501.
[61] G. J. Martyna, M. L. Klein, M. Tuckerman, *J. Chem. Phys.* **1992**, *97*, 2635–2643.
[62] D. J. Evans, B. L. Holian, *J. Chem. Phys.* **1985**, *83*, 4069–4074.
[63] G. Mondanelli, A. Coletti, F. A. Greco, M. T. Pallotta, C. Orabona, A. Iacono, M. L. Belladonna, E. Albini, E. Panfili, F. Fallarino, M. Gargaro, G. Manni, D. Matino, A. Carvalho, C. Cunha, P. Maciel, M. Di Filippo, L. Gaetani, R. Bianchi, C. Vacca, I. M. Iamandii, E. Proietti, F. Boscia, L. Annunziato, M. Peppelenbosch, P. Puccetti, P. Calabresi, A. Macchiarulo, L. Santambrogio, C. Volpi, U. Grohmann, *Proc. Natl. Acad. Sci. USA* **2020**, *117*, 3848–3857.

Manuscript received: June 19, 2021
Revised manuscript received: August 3, 2021
Accepted manuscript online: August 5, 2021
Version of record online: August 27, 2021